ACS APPLIED MATERIALS & INTERFACES

Research Article

www.acsami.org

Delicate Refinement of Surface Nanotopography by Adjusting TiO_2 Coating Chemical Composition for Enhanced Interfacial Biocompatibility

Xiaobing Zhao,[†,‡] Guocheng Wang,*[,‡] Hai Zheng,[†] Zufu Lu,[‡] Xia Zhong,[§] Xingbao Cheng,[†] and Hala Zreiqat*[,‡]

[†]School of Materials Science and Engineering, Changzhou University, Changzhou 213164, China

[‡]Biomaterials and Tissue Engineering Research Unit, School of AMME, and [§]School of Chemical and Biomolecular Engineering, The University of Sydney, Sydney 2006, Australia

ABSTRACT: Surface topography and chemistry have significant influences on the biological performance of biomedical implants. Our aim is to produce an implant surface with favorable biological properties by dual modification of surface chemistry and topography in one single simple process. In this study, because of its chemical stability, excellent corrosion resistance, and biocompatibility, titanium oxide (TiO_2) was chosen to coat the biomedical Ti alloy implants. Biocompatible elements (niobium (Nb) and silicon (Si)) were introduced into TiO_2 matrix to change the surface chemical composition and tailor the thermophysical properties, which in turn leads to the generation of topographical features under specific thermal history of plasma spraying. Results demonstrated that introduction of Nb_2O_5 resulted in the formation of $Ti_{0.95}Nb_{0.95}O_4$ solid solution and led to the generation of nanoplate network structures on the composite coating surface. By contrast, the addition of SiO_2 resulted in a hairy nanostructure and coexistence of rutile and quartz phases in the coating. Additionally, the introduction of Nb_2O_5 enhanced the corrosion resistance of TiO_2 coating, whereas SiO_2 did not exert much effect on the corrosion behaviors. Compared to the TiO_2 coating, TiO_2 coating doped with Nb_2O_5 enhanced primary human osteoblast adhesion and promoted cell proliferation, whereas TiO_2 coatings with SiO_2 were inferior in their bioactivity, compared to TiO_2 coatings. Our results suggest that the incorporation of Nb_2O_5 can enhance the biological performance of TiO_2 coatings by changing the surface chemical composition and nanotopgraphy, suggesting its potential use in modification of biomedical TiO_2 coatings in orthopedic applications.

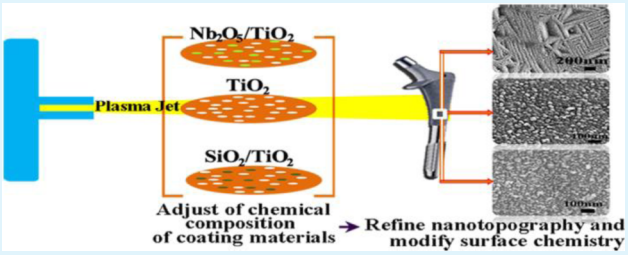

KEYWORDS: *surface chemistry and topography, titanium oxide, nanostructure, niobium, osteoblast, rapid solidification*

INTRODUCTION

Titanium and its alloy (Ti-6Al-4V) are promising metal materials for orthopedic applications due to their excellent mechanical properties.[1] They have been used as artificial hip joint, bone plates and dental implants. However, the main drawback of Ti-6Al-4V implants is their suboptimal surface properties which result in poor interfacial bonding between the host bone and the implant,[2] which poses a risk of the premature failure of the device. The success of orthopedic implants depends on strong anchorage of the device material in bone tissue. Various biomaterials modifications have been applied in an attempt to enhance bone formation, but to date none forms a stable interface with the strength required to support functional loading and to improve the implant bioactivity and osseointegration.[3,4]

Surface chemistry and topography are two of the most important properties that determine the biological performance of the implants.[5,6] An important factor in selecting orthopedic implant material, therefore, is identifying the correct chemistry and topography to support or stimulate an appropriate host response. Chemically, the surface of the implant can be modified by incorporating biocompatible trace elements, which are essential for normal bone metabolism.[7] Trace-elements including Sr, Si, and Zn, have been utilized and their beneficial effects on the improvement of biological performance of implant have been proved.[8−10]

Physically, the surface topography at both micro- and nanoscales plays a major role in modulating the interactions of implants and cells/tissues, thus influencing the osseointegration of the implants.[11,12] Surfaces with micrometer-sized roughness not only have positive effects on the cell attachment, proliferation and differentiation,[13] but also present a large surface area for the anchorage of newly formed bone, compared to that of a smooth surface, thereby enhancing the osseointegration of the implant.[14,15] The beneficial effects of nanotopography have been also reported by many researchers.

Received: June 14, 2013
Accepted: August 6, 2013
Published: August 6, 2013

   dx.doi.org/10.1021/am402319a | ACS Appl. Mater. Interfaces 2013, 5, 8203−8209

Webster et al.[16] reported that the nanoscale topographical features can increase the surface energy and promote selective adsorption of some proteins, resulting in enhanced biomaterial osseointegration by improving cell adhesion, migration, proliferation, and differentiation.[3] Although these methods have led to improvements, sufficient osseointegration has still not been realized. To gain the maximum enhancement of the biological performance of the implant, biomaterial scientists have been trying to employ surface modification techniques that involve both surface chemistry and surface topography (at the micro- and nanoscale) in one simple and single process.[17,18]

Plasma spraying technique has the potential to achieve dual surface modification of implants due to its high temperature characteristic and the superhigh cooling rate.[19] Plasma spray yields temperatures up to 12 000 K in the core region of a plasma jet, with which various ceramic powders can be melted down and deposited onto the substrates. Moreover, a cooling rate up to 1×10^6 to 1×10^7 K s^{-1} during plasma spraying process is able to lead to the occurrence of ultrarapid quenching of the melts during solidification. Under such thermal conditions, the growth of crystallites is strongly suppressed, leading to the formation of some nonequilibrium phases and unique fine structures.[20] In our previous study, we succeeded in the production of nanostructured coatings using conventional powders based on this specific thermal history of plasma spraying.[12] We also demonstrated that the obtained hybrid nano/microstructures enhanced the cellular activity and promoted bone healing.[12]

TiO_2 coating has been proposed to be a substitute for the currently used biomedical coatings due to its chemical stability, nontoxicity and biocompatibility.[21,22] However, the TiO_2 coating is incapable of inducing new bone formation at the implant surface, rendering it suboptimal for use as a coating for orthopedic implants. The goal of the present study is to improve the bioactivity of the TiO_2 coating using dual surface modification technique. To change the surface chemistry, we introduced the bioactive trace element Si and the biocompatible Nb elements into TiO_2 coatings through the incorporation of SiO_2 and Nb_2O_5. The effects of Si elements in enhancing the bioactivity of biomaterials have been well-documented.[23] Nb has recently received great attention in the biomedical field either as alloy elements to improve the corrosion resistance of some metal implants or as a second phase for enhancing the biocompatibility of some biomaterials.[24−28] Nb_2O_5 has also been studied for orthopedic application showing good corrosion resistance and biocompatibility.[29,30] Ding et al.[31] produced Nb doped TiO_2 nanotubes on the surface of a Ti35Nb alloy, and demonstrated that Nb enhanced the in vitro bioactivity of TiO_2 by promoting mesenchymal stem cell adhesion and inducing the formation of the extracellular matrix (ECM).

Because of the potentials in producing adjustable nano/micro topographies, plasma spraying technique was utilized in this study. We envisaged that the addition of SiO_2 and Nb_2O_5 would also adjust the fine structures of the resultant coatings as it changed the thermophysical properties of TiO_2 coatings which in turn influenced the solidification process. In this study, we evaluated the corrosion resistance and cytocompatibility of the SiO_2 -and Nb_2O_5 doped TiO_2 coatings with pure TiO_2 coatings as a control group.

EXPERIMENTAL SECTION

Coating Fabrication. TiO_2 (P25, Deggusa; 30 nm, ≥99.6%), Nb_2O_5 (Shanghai CNPC powder material Co., Ltd., China; 10 μm, ≥99.9%), and SiO_2 (Shanghai Ruiyu optical and electrical materials Co., Ltd., China; 20 μm, ≥99.2%) powders were used as feedstocks. The composite Nb_2O_5/TiO_2 powders were produced by mixing Nb_2O_5 and TiO_2 with a proportion of 1:1 by weight in absolute ethanol, followed by ball-milling, drying and sieving. The process for mixing the powders is briefly described as follows: 100g powders were placed in the ball milling tank, and then 50 mL of ethanol and 10 mL of poly(vinylalcohol) (PVA) solution (5 wt %) were added into the tank. After thorough mixing by in the ball mill for 2 h, powders were dried at 80 °C for 24 h. The powders were finally sieved using 80 mesh sieves. Those below 80 mesh were used for plasma spraying; 50 wt % SiO_2/TiO_2 powders were prepared in the same way.

Coatings were deposited on commercial cp-Ti discs with a dimension of 10 mm × 10 mm × 1 mm using an atmospheric plasma spraying system (9M, Sulzer Metco, USA). Before plasma spraying, the cp-Ti discs were ultrasonically cleaned in absolute ethanol and grit-blasted with brown corundum. The spraying parameters are listed in Table 1. The as-sprayed coatings were ultrasonically cleaned in acetone and deionized water.

Table 1. Spraying Parameters of Atmospheric Plasma Spraying

primary gas (Ar) flow rate (slpm[a])	40
secondary gas (H_2) flow rate (slpm)	12
spraying power (KW)	42
spraying distance (mm)	100
powder feed rate (g/min)	20

[a]slpm: standard liter per minute.

The phase composition of the coatings was characterized by X-ray diffraction (XRD) using a Shimadzu 6000 diffractometer equipped with Cu Kα radiation (λ = 1.5418 Å) at a step size of 0.02°. Data were obtained from 20 to 80° 2θ at a scanning rate of 4° min^{-1}. Surface morphologies of the coatings were examined by field emission scanning electron microscopy (FESEM, Zeiss Ultra Plus). The chemical composition of the coatings was determined by energy-dispersive X-ray spectrometry (EDS, Oxford). The Nb and Si content in the coatings (R) was evaluated by the equation R (wt %) = (M/(M + Ti) (M = Nb or Si) according to the EDS data, with comparison to the theoretical values equal to original values of Nb and Si relative content in the composite powders. The cross-sectional morphologies of the coatings were observed by SEM (Hitachi S3800). The bonding strength was evaluated according to the ASTM C-633-79 procedure. Briefly, coatings with a thickness around 380 μm were deposited onto cp-Ti rods with a diameter of 25.4 mm. E-7 adhesive glue was applied to adhere the coated cp-Ti rods with the uncoated ones before tensile testing performed using a universal testing machine (Instron-5592, SATEC, USA) and four samples were tested independently. More details about the bonding strength measurement can be found in our previous work.[32] Data were presented as means ± standard deviation (SD).

Electrochemical Measurement. The corrosion behavior of the as-sprayed coatings was evaluated by electrochemical workstation (CS400, China) in simulated body fluid (SBF) at 37 °C. A standard three-electrode cell, using copper as an auxiliary electrode and saturated calomel electrode (SCE) as a reference electrode, was utilized for the electrochemical measurement. When the open-circuit potential became almost steady, the test pieces with approximate 1 cm^2 exposed to the electrolyte were scanned at potential sweep rate of 5 mV s^{-1}.

Cell Culture. The procedures of cell culture in this work are same as those used in our previous works.[9−11,32] Briefly, primary human osteoblasts (HOBs) were first isolated from normal human trabecular bones, with a permission to use discarded human tissue was granted by

the Human Ethics Committee of the University of Sydney and informed consent. Then, the isolated HOBs were cultured at 37 °C in an atmosphere of 5% CO_2 and medium was refreshed every three days. Those cells at passage 3 were used in the following experiments. 0.5 mL cell suspension with a density of 8.0×10^4 cells per ml was added into each well of a 24 well tissue culture plate containing coating samples. After 2 and 24 h of culturing, HOBs were fixed in a 4% paraformaldehyde solution. For fluorescence microscopy observation, HOBs cultured on the coatings were stained with rhodamine phalloidin (Invitrogen Detection Technologies, USA) at room temperature for 40 min, and rinsed with PBS. The cytoskeleton of HOBs was then visualized using a Leica TCS SPII Multiphoton Microscope. For SEM observation, coatings with HOBs were dehydrated in a series of graded ethanol solution, and dried in hexamethyldisilizane for 3 min. The morphology of the HOBs cultured on the coating surface was observed by a Zeiss ultra plus field-emission scanning electron microscope after gold sputtering.

Cell proliferation was tested using alamarBlue assay (Invitrogen, USA). Four replicates per group were used for statistical analysis. After culturing for 3, 7, and 14 days, culture medium was replaced by 1 mL fresh medium with 10% alamarBlue. After incubation for 5 h, 100 μL alamarBlue-contained medium was transferred to a 96-well plate to measure its optical density by an enzyme labeling instrument (MULTISKAN EX, Thermo Elecron Corporation, China) at extinction wavelengths of 570 and 600 nm. Accumulation of the reduced alamarBlue by the vital HOBs indicating the cellular proliferation was calculated in accordance with instruction manual of alamarBlue assay. More details about the proliferation test are available in our previous study.[33]

SPSS 17.0 program was used to perform statistical analysis. The data were expressed as Mean + SD. To evaluate the homogeneity of variance, Levene's test was carried out. If the tested groups have homogeneous variance, Tukey HSD post hoc test will be used, otherwise, Tamhane's T2 post hoc will be employed. The difference between means will be considered significant if the p-value of less than 0.05.

RESULTS

Phase Composition. Figure 1 shows the XRD patterns of the as-sprayed TiO_2, Nb_2O_5 doped TiO_2 and SiO_2 doped TiO_2

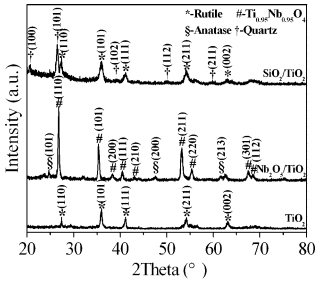

Figure 1. XRD patterns of the TiO_2, Nb_2O_5/TiO_2, and SiO_2/TiO_2 coatings.

coatings. The TiO_2 coating is mainly composed of rutile (JCPDS No.: 21−1276). 50%Nb_2O_5/TiO_2 composite coating consists of $Ti_{0.95}Nb_{0.95}O_4$ (JCPDS No.: 47−0024) solid solution and a small amount of anatase phase. In general, the addition of Li^+, Cu^{2+}, Co^{2+}, Fe^{3+}, and Mn^{4+} in the forms of oxides or fluorides into TiO_2 can assist the phase transformation from anatase to rutile. However, it has been reported that although Nb^{5+}, PO_4^{3-}, and SO_4^{2-} can inhibit the phase transformation,[34−36] it is reasonable to attribute the existence of small amount of anatase to the doping of Nb_2O_5. In contrast, 50%SiO_2/TiO_2 composite coating contains separated rutile and quartz (JCPDS No.: 46−1045) phases with a small amount of glass phase shown in the broadening of the diffraction peaks.

Surface Morphologies. SEM micrographs of the TiO_2, Nb_2O_5/TiO_2, and SiO_2/TiO_2 coatings are displayed in Figure 2. All coatings exhibit rough surface where many splats are

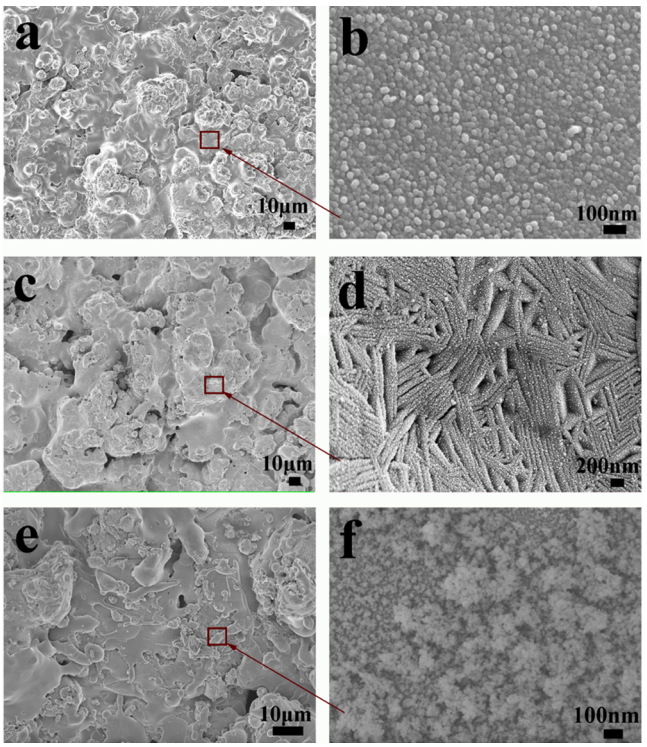

Figure 2. SEM micrographs of the (a, b) TiO_2, (c, d) Nb_2O_5/TiO_2, and (e, f) SiO_2/TiO_2 coatings (Images b, d, and f are under higher magnifications).

observed resulting from the impingement of the melted powders on the existing coating layers (Figure 2a, c, and e). This is one of the typical characteristics of plasma sprayed coatings.[37] Prominent differences in the structures at nanoscale can be observed among these three types of coatings (Figure 2b, d, and f). The nanostructures of TiO_2 coating are composed of grains with a size less than 50 nm. It is noted that nanoplate network structures, obviously different from the one formed on the TiO_2 coatings (Figure 2b), are formed on the surface of the Nb_2O_5/TiO_2 composite coatings, indicating the pronounced influence of Nb_2O_5 on the topography of TiO_2 coatings (Figure 2d). By contrast, nanostructures with irregular hairy protrusions are formed on the surface of the SiO_2/TiO_2 coating (Figure 2f).

Figure 3a and b present EDS spectra of the Nb_2O_5/TiO_2 and SiO_2/TiO_2 coatings and Figure 3c displays the weight ratios of Nb/(Nb+Ti) and Si/(Si+Ti) in the coatings calculated according to the EDS data. As expected, Nb is detected in the Nb_2O_5/TiO_2 coating (Figure 3a) and Si in the SiO_2/TiO_2 coating (Figure 3b). From Figure 3c, it can be seen that the calculated Nb/Ti is comparable to the theoretical value, while the calculated Si/Ti is lower than the theoretical value. This indicates that there is no loss of Nb but a small amount of Si is lost during the plasma spraying process.

Cross-Sectional Morphologies. Figure 4 shows the cross-sectional morphologies of the TiO_2, Nb_2O_5/TiO_2 and SiO_2/TiO_2 coatings. All the three types of coatings have a similar thickness about 40 μm. Cross sections demonstrated that the

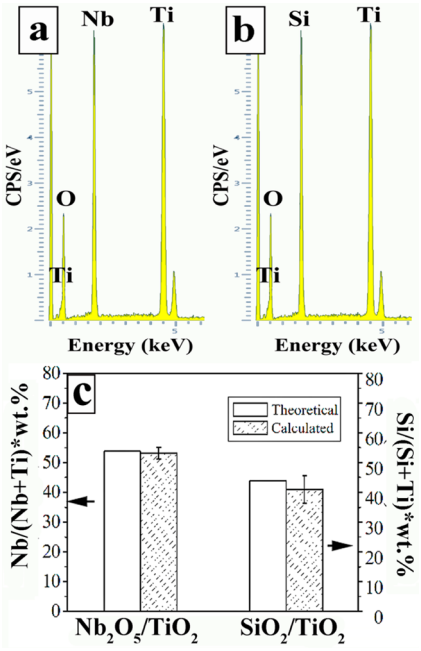

Figure 3. EDS spectra of the (a) Nb_2O_5/TiO_2 and (b) SiO_2/TiO_2 coatings, (c) relative content of Nb and Si in coatings calculated from EDS data.

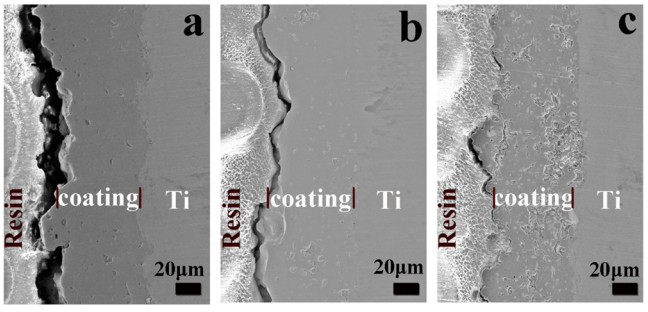

Figure 4. Cross-sectional morphologies of the (a) TiO_2, (b) Nb_2O_5/TiO_2, and (c) SiO_2/TiO_2 coatings.

TiO_2 and Nb_2O_5/TiO_2 coatings are smooth and dense (Figure 4a and b), while many voids and pits are found distributed throughout the SiO_2/TiO_2 coating (Figure 4c), indicating the less integrity of the SiO_2/TiO_2 coating, compared to that of the Nb_2O_5/TiO_2 coating. No gap is visible between the coating and Ti alloy substrates for the TiO_2 and Nb_2O_5/TiO_2 coatings (Figure 4a and b), whereas some gaps are visible at the coating/Ti alloy interface (Figure 4c), indicating that the interfacial bonding of the TiO_2 and Nb_2O_5/TiO_2 coating are better than that of the SiO_2/TiO_2 coating. Figure 5 presents the bonding strength of the TiO_2, Nb_2O_5/TiO_2, and SiO_2/TiO_2 coatings. The bonding strength between the Nb_2O_5 coating and cp-Ti substrate is 39.5 ± 4.6 MPa which is significantly higher than that of the TiO_2 (23.5 ± 4.6 MPa, $p = 0.007$) and SiO_2/TiO_2 (11.5 ± 3.3 MPa, $p = 0.001$) coatings.

Corrosion Resistance. Figure 6 presents the potentiodynamic polarization curves of the as-sprayed TiO_2, Nb_2O_5/TiO_2 and SiO_2/TiO_2 coatings in SBF solution at 37 °C. The corrosion potential (E_{corr}) of the TiO_2, Nb_2O_5/TiO_2, and SiO_2/TiO_2 coatings is about −347, −312, and −352 mV, respectively. The electrode potential is an indicator of corrosion activity; the more negative the potential is, the worse the corrosion

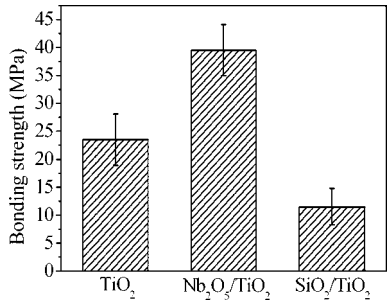

Figure 5. Interficial bonding strength of the TiO_2, Nb_2O_5/TiO_2 and SiO_2/TiO_2 coatings.

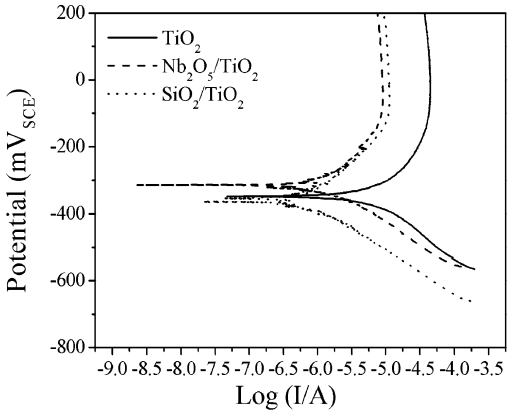

Figure 6. Potentiodynamic polarization curves of the TiO_2, Nb_2O_5/TiO_2, and SiO_2/TiO_2 coatings.

resistance will be. The corrosion current density (I_{corr}) of the Nb_2O_5/TiO_2 coating is around 1.56 $\mu A/cm^2$, which is lower than that of the TiO_2 (2.25 $\mu A/cm^2$) and SiO_2/TiO_2 coatings (2.51 $\mu A/cm^2$) indicating that the Nb_2O_5/TiO_2 coating has a slower corrosion rate. All together, results of electrochemical analysis suggest that the Nb_2O_5/TiO_2 coating has better corrosion resistance compared to the TiO_2 and SiO_2/TiO_2 coatings. However, no significant improvement can be observed on the SiO_2/TiO_2 coating, compared to the TiO_2 coating.

Cell Attachment and Proliferation. The initial adhesive interaction between the cells and biomaterials is a key regulator of cellular proliferation, differentiation, activation and migration. Confocal and SEM images of the HOBs seeded on the surface of the TiO_2, Nb_2O_5/TiO_2 and SiO_2/TiO_2 coatings for 2 and 24 h are depicted in Figures 7 and 8. After 2 h of culture, HOBs seeded on the surfaces of the TiO_2 and Nb_2O_5/TiO_2 coatings are more voluminous and spread out (Figure 7a, b (confocal) and Figure 8a−d (SEM)), compared to a less spread out morphology for the HOBs on the SiO_2/TiO_2 coating (Figures 7c and 8e, f). Indeed, the proliferation results (Figure 9) reflects a similar trend whereby at day 3 in culture, HOBs proliferation rate on the Nb_2O_5/TiO_2 coatings is higher than that on the TiO_2 and SiO_2/TiO_2 coatings. By day 7, the HOBs proliferation rates on both TiO_2 and Nb_2O_5/TiO_2 coatings is similar, albeit less than that for the cells on the SiO_2/TiO_2 surface. At day 14, the cell proliferation on the Nb_2O_5/TiO_2 coating is significantly higher compared to that for the TiO_2 coating. These results suggest the enhanced bioactivity of the TiO_2 coating by the addition of Nb_2O_5 and not by the incorporation of SiO_2.

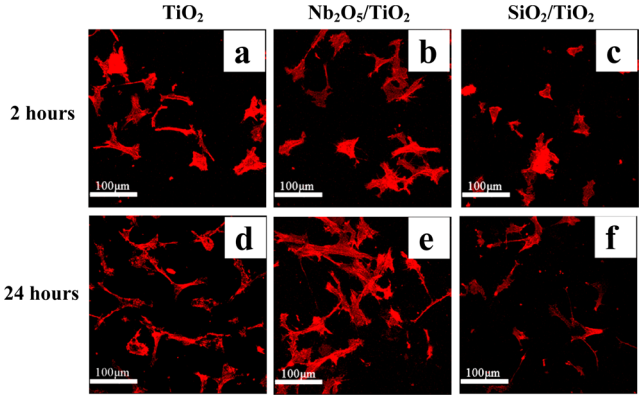

Figure 7. Confocal images of HOBs seeded on the surface of the TiO_2, Nb_2O_5/TiO_2, and SiO_2/TiO_2 coatings for 2 and 24 h.

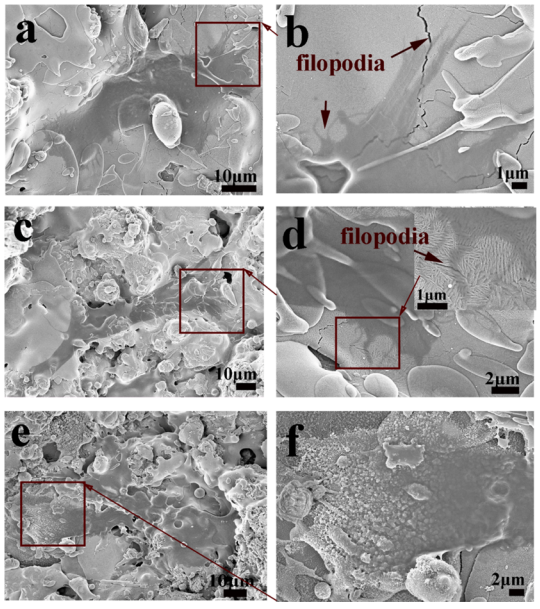

Figure 8. SEM micrographs of HOBs cultured on the (a, b) TiO_2, (c, d) Nb_2O_5/TiO_2, and (e, f) SiO_2/TiO_2 coatings for 2 h (b, d, and f are enlarged images from the framed areas).

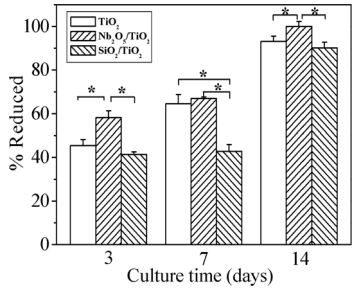

Figure 9. Proliferation of HOBs cultured on TiO_2, Nb_2O_5/TiO_2 and SiO_2/TiO_2 coatings after 3, 7, and 14 days, $*p < 0.05$.

DISCUSSION

Biomaterials surfaces play an ultimate role in determining their success as the initial biological reactions occur on the implant surface.[5,6] To develop biomaterials with highly bioactive surfaces, various surface modification/coating methods have been investigated. In the present study, we adapted a simple and cost-effective surface modification technique that can delicately adjust the surface ultrastructure while altering the surface chemistry in one simple and single process.

Plasma spraying is a well-established coating technique which has been widely used in various industry fields including corrosion protection, wear-resistant, thermal barrier and medical implants.[38,39] Conventional air plasma spraying has long been considered to be an effective rapid solidification technique, since it allows continuous quenching during coating.[40] The rapid solidification effect of plasma spraying was observed by Moss[41] in the form of high super saturation of vanadium in aluminum. Since then, it has been widely used to produce metal and alloy coatings with unique nonequilibrium phases and structures. However, this effect has not provoked much interest in producing ceramic coatings with specific phase and fine structures. We previously utilized conventional feedstocks (with a particle size more than 100 μm) to produce zirconia ceramic coatings, which in turn led to the generation of nanostructured surfaces consisting of nanograins of less than 50 nm in size.[32] The formation of this nanostructure surface was due to the recrystallization during the rapid solidification process,[12] which is influenced by many factors including the temperature of the substrate, processing parameters of the plasma spraying and the additional cooling conditions.[39] Therefore, the nonequilibrium phase and structure can be adjusted by changing processing parameters, preheating the substrates and utilizing the additional cooling apparatus. Besides these factors, the thermophysical property of the spraying material itself is another important factor that can refine the structure and properties of the coatings.

In this study, we succeeded in controlling the fine structures of the plasma-sprayed coatings by changing the chemical compositions of the spraying materials. The three types of coatings (TiO_2, Nb_2O_5/TiO_2 and SiO_2/TiO_2) were produced by the same spraying parameters. However, they displayed different surface fine structures, among which the nanoplate network structure formed by the introduction of Nb_2O_5 in TiO_2 coatings are totally different from the other two nanostructures. Under the same spraying conditions, the thermal history that these three coatings underwent from exterior environment should be the same; therefore, the reason for the differences in the fine structures should lie in the material itself, namely, the difference in thermodynamic properties caused by the introduction of Nb_2O_5 and SiO_2.

During the solidification process of the plasma sprayed coatings, the melt recrystallizes under nonequilibrium condition. This recrystallization is influenced by the thermal-physical properties of the coating materials and any physical and chemical reactions during the solidification, causing changes in the heat. For Nb_2O_5 doped TiO_2 coatings, XRD data demonstrated that they were mainly composed of $Ti_{0.95}Nb_{0.95}O_4$, a newly formed solid solution (Figure 1). The formation of solid solution is the result of the atom migration, which requires energy adsorption and in turn leads to the change in heat, which influences the recrystallization process during the solidification. This possibly accounts for the specific fine structure of the Nb_2O_5 doped TiO_2 coatings. Further studies are planned to explore the exact mechanism(s) by which the oxide dopants influence the formation of the nanostructures.

Although there were some differences in the nanostructure, all three types of coatings exhibited micrometer-rough surfaces (Figure 2a, c, e), one of the characteristics of plasma-sprayed coatings.[42,43] The surface roughness (Ra) values of the TiO_2,

Nb_2O_5/TiO_2, and SiO_2/TiO_2 coatings measured by surface profilometry are 7.18 ± 0.70 μm, 10.17 ± 0.62 μm, and 7.84 ± 0.98 μm, respectively. Therefore, the Nb_2O_5 doped TiO_2 coatings not only has a modified surface chemistry and delicate refinement of nanostructure but also has a microstructure topography.

Both chemical composition and nanotopographical features can influence the cell behaviors including attachment, adhesion, proliferation and differentiation.[12,44] In the present study, we demonstrated the bioactivity of the Nb_2O_5 doped TiO_2 coatings as reflected in the enhanced HOBs adhesion and proliferation compared to that of both the pure TiO_2 and the SiO_2 doped coatings. It is plausible to suggest that the bioactivity of the Nb_2O_5/TiO_2 coatings is ascribed to its specific nanostructure (topography effect) as well as to the presence of Nb (chemistry) in the coating surface. The effect of Nb on the cellular responses has been previously reported whereby Ding et al.[31] found that Nb doped TiO_2 nanotubes had an enhanced in vitro bioactivity by promoting the adhesion of the mesenchymal stem cell adhesion and the formation of ECM, compared to the undoped TiO_2 nanotubes.

While the beneficial effects of Si have been reported and utilized by many researchers,[45,46] in the present study, SiO_2 doped TiO_2 coatings did not show an enhanced cytocompatibility, compared to the pure TiO_2 coatings, possibly because of the form of Si present.[47] The Si in the SiO_2/TiO_2 coatings is in the form of a well-crystallized quartz phase; a stable phase with poor degradability. The concentration of Si ions released from the SiO_2/TiO_2 coatings after soaking in phosphate-buffered saline solution is 4.76 ppm, a far less concentration than the reported one required to enhance the activity of cells.[48−51] Sun et al.[52] reported that Si ion released from plasma-sprayed Ca_2SiO_4 coatings induced osteoblast proliferation and differentiation. However, the reported Si concentration was 75 ppm, much higher than that released from the SiO_2/TiO_2 coatings in our study.

Nb_2O_5 doped TiO_2 coatings have better interfacial bonding and corrosion resistance compared to the pure TiO_2 coatings and the SiO_2 doped TiO_2 coatings (Figures 4−6). High interfacial bonding strength between the coating and the underlying substrates can avoid the issue of coating delamination, ensuring the long-term stability of the implants. The coefficients of thermal expansion (CTE) of the coating and substrates are of significant importance to the interfacial bonding strength. The match of the CTE between the Ti substrate ($9.7−9.9 \times 10^{-6}$ K^{-1})[53] and TiO_2 coating ($8.0−10.0 \times 10^{-6}$ K^{-1})[54] leads to the higher interfacial bonding strength of the TiO_2 coating. Because CET of the Nb_2O_5 coating is $5.3−5.9 \times 10^{-6}$ K^{-1},[55] lower than that of Ti substrates, the enhancement of bonding strength by the addition of Nb_2O_5 was thought to result from the formation of the solid solution whose CET is possibly closer to that of the Ti substrate. By contrast, the CET of SiO_2 (5.5×10^{-7} K^{-1})[54] is much lower than that of Ti substrates and TiO_2, such difference of 1 order of magnitude is the one of the most important reasons for the inferior interfacial bonding of SiO_2 doped coatings.

The corrosion resistance is another confounding factor contributing to the ultimate behavior of biomedical implants, affecting their stability and biosafety. The pores, microcracks in the coating and the poor interfacial bonding between the coating and the substrate can accelerate the corrosion, causing serious problems to the implants. The local defects in the coatings can also form direct paths between a corrosive environment and the underlying coating, leading to localized galvanic attack and corrosion beneath coating layers.[56] Therefore, better integrity of the pure TiO_2 and the Nb_2O_5 doped coatings accounts for their enhanced corrosion resistance, compared to that of the SiO_2 doped TiO_2 coatings. The formation of the $Ti_{0.95}Nb_{0.95}O_4$ solid solution is another possible contributing factor in the improvement of the corrosion resistance. Similar effect of solid solution on the corrosion resistance was also reported by other researchers.[57−59]

CONCLUSION

In this study, we tailored the surface fine structures of TiO_2 coatings by adjusting the chemical composition of the coating, utilizing the unique characters of plasma spraying technique; the rapid solidification effect. All coatings presented micro-rough surface structures, but differ in their nanostructures. The pure TiO_2 coatings exhibited a nanostructure with nano grain with a size less than 50 nm. By contrast, the nanostructure of the Nb_2O_5 doped TiO_2 coating was constructed by nanosized plates. However, the addition of SiO_2 in TiO_2 coating changed the original nanostructure of the pure TiO_2 coatings. These differences are thought to be caused by the changes in the thermo-physical properties resulting from the adjustment of chemical composition of the coatings. Nb_2O_5 doped TiO_2 coatings showed better in vitro bioactivity, compared to the pure TiO_2- and SiO_2 doped TiO_2 coatings; possibly attributed to the changes in both surface chemistry and surface nanotopography. Additionally, Nb_2O_5 doped TiO_2 coatings presented better interfacial adhesion and enhanced corrosion resistance. These results indicate that Nb_2O_5 doped TiO_2 coatings have potential for applications as biomedical coatings in orthopedic implants. Our study validated the feasibility of realizing both chemical and nanotopographical modification via well-established plasma spraying by simply adjusting the chemical composition of coatings, which may expand the application scope of plasma spray in the biomedical field.

AUTHOR INFORMATION

Corresponding Author

*E-mail: lanceplus2@gmail.com (G.W.); hala.zreiqat@sydney.edu.au (H.Z.). Tel.: +34 943005321 (G.W.); +61 2 9351 2392 (H.Z.).

Notes

The authors declare no competing financial interest.

ACKNOWLEDGMENTS

The authors give thanks to Jiangsu Overseas Research & Training Program for University Prominent Young & Middle-aged Teachers and Presidents. The authors acknowledge the Australia National Health and Medical Research Council (NHMRC) for funding this research. The authors also acknowledge the Australia National Health and Medical Research Council, Rebecca Cooper Foundation. The authors thank Australian Centre for Microscopy & Microanalysis for their assistance in Micro/Nano analysis.

REFERENCES

(1) Niinomi, M. *J. Artif. Organs* **2008**, *11*, 105−110.
(2) Gomez-Vega, J. M.; Saiz, E.; Tomsia, A. P. *J. Biomed. Mater. Res.* **1999**, *46*, 549−559.
(3) Ehrenfest, D. M. D.; Coelho, P. G.; Kang, B. S.; Sul, Y. T.; Albrektsson, T. *Trends Biotechnol.* **2010**, *28*, 198−206.

(4) Coelho, P. G.; Granjeiro, J. M.; Romanos, G. E.; Suzuki, M.; Silva, N. R. F.; Cardaropoli, G.; Van, P. V.P.; Lemons, J. E. *J. Biomed. Mater. Res., Part B* **2009**, *88*, 579−596.
(5) Smith, D. C.; Pilliar, R. M.; Chernecky, R. *J. Biomed. Mater. Res.* **1991**, *25*, 1045−1068.
(6) Kieswetter, K.; Schwartz, Z.; Dean, D. D.; Boyan, B. D. *Crit. Rev. Oral Biol. Med.* **1996**, *7*, 329−345.
(7) Howlett, C. R.; Zreiqat, H.; Wu, Y.; McFall, D. W.; McKenzie, D. R. *J. Biomed. Mater. Res.* **1999**, *45*, 345−354.
(8) Zhang, W.; Wang, G.; Liu, Y.; Zhao, X.; Zou, D.; Zhu, C.; Jin, Y.; Huang, Q.; Sun, J.; Liu, X.; Jiang, X.; Zreiqat, H. *Biomaterials* **2013**, *34*, 3184−3195.
(9) Wang, G.; Lu, Z.; Liu, X.; Zhou, X.; Ding, C.; Zreiqat, H. *J. R. Soc. Interface* **2011**, *8*, 1192−1203.
(10) Wang, G.; Lu, Z.; Dwarte, D.; Zreiqat, H. *Mater. Sci. Eng., C* **2012**, *32*, 1818−1826.
(11) Wang, G.; Lu, Z.; Xie, K. Y.; Lu, W. Y.; Roohani-Esfahani, S. I.; Kondyurin, A.; Zreiqat, H. J. *Mater. Chem.* **2012**, *22*, 19081−19087.
(12) Wang, G.; Liu, X.; Zreiqat, H.; Ding, C. *Colloids Surf., B* **2011**, *86*, 267−274.
(13) Zhao, G.; Raines, A. L.; Wieland, M.; Schwartz, Z.; Boyan, B. D. *Biomaterials* **2007**, *28*, 2821−2829.
(14) Rønold, H. J.; Ellingsen, J. E. *Biomaterials* **2002**, *23*, 4211−4219.
(15) Suzuki, K.; Aoki, K.; Ohya, K. *Bone* **1997**, *21*, 507−514.
(16) Webster, T. J.; Siegel, R. W.; Bizios, R. *Biomaterials* **1999**, *20*, 1221−1227.
(17) Variola, F.; Yi, J. H.; Richert, L.; Wuest, J. D.; Rosei, F.; Nanci, A. *Biomaterials* **2008**, *29*, 1285−1298.
(18) Xia, W.; Lindahl, C.; Lausmaa, J.; Borchardt, P.; Ballo, A.; Thomsen, P.; Engqvist, H. *Acta Biomater.* **2010**, *6*, 1591−1600.
(19) Chu, P. K. *IEEE Trans. Plasma Sci.* **2007**, *35*, 181−187.
(20) Trifa, F. I.; Montavon, G.; Coddet, C.; Nardin, P.; Abrudeanu, M. *Mater. Charact.* **2005**, *54*, 157−175.
(21) Geetha, M.; Singh, A. K.; Asokamani, R.; Gogia, A. K. *Prog. Mater. Sci.* **2009**, *54*, 397−425.
(22) Shao, H.; Yu, C.; Xu, X.; Wang, J.; Zhai, R.; Wang, X. *Appl. Surf. Sci.* **2010**, *257*, 1649−1654.
(23) Shibli, S. M. A.; Mathai, S. *J. Mater. Sci.: Mater. Med.* **2008**, *19*, 2971−2981.
(24) Karlinsey, R. L.; Hara, A. T.; Yi, K.; Duhn, C. W. *Biomed. Mater.* **2006**, *1*, 16−23.
(25) Eisenbarth, E.; Velten, D.; Breme, J. *Biomol. Eng.* **2007**, *24*, 27−32.
(26) Wang, Y. B.; Zheng, Y. F. *Mater. Lett.* **2009**, *63*, 1293−1295.
(27) Zhou, F. Y.; Wang, B. L.; Qiu, K. J.; Lin, W. J.; Li, L.; Wang, Y. B.; Nie, F. L.; Zheng, Y. F. *Mater. Sci. Eng., C* **2012**, *32*, 851−857.
(28) Jirka, I.; Vandrovcová, M.; Frank, O.; Tolde, Z.; Plšek, J.; Luxbacher, T.; Bačáková, L.; Starý, V. *Mater. Sci. Eng., C* **2013**, *33*, 1636−1645.
(29) Velten, D.; Eisenbarth, E.; Schanne, N.; Breme, J. *J. Mater. Sci.: Mater. Med.* **2004**, *15*, 457−461.
(30) Ramírez, G.; Rodil, S. E.; Arzate, H.; Muhl, S.; Olaya, J. J. *Appl. Surf. Sci.* **2011**, *257*, 2555−2559.
(31) Ding, D.; Ning, C.; Huang, L.; Jin, F.; Hao, Y.; Bai, S.; Li, Y.; Li, M.; Mao, D. *Nanotechnology* **2009**, *20*, 305103−305108.
(32) Wang, G.; Meng, F.; Ding, C.; Chu, P. K.; Liu, X. *Acta Biomater.* **2010**, *6*, 990−1000.
(33) Wang, G.; Liu, X.; Gao, J.; Ding, C. *Acta Biomater.* **2009**, *5*, 2270−2278.
(34) Hirano, M.; Ichihashi, Y. *J. Mater. Sci.* **2009**, *44*, 6135−6143.
(35) Criado, B. J.; Real, C. *J. Chem. Soc., Faraday Trans. 1* **1983**, *79*, 2765−2771.
(36) Arbiol, J.; Cerdà, J.; Dezanneau, G.; Cirera, A.; Peiró, F.; Cornet, A.; Morante, J. R. *J. Appl. Phys.* **2002**, *92*, 853−861.
(37) Kang, C. W.; Ng, H. W. *Surf. Coat. Technol.* **2006**, *200*, 5462−5477.
(38) Aruna, S. T.; Balaji, N.; Shedthi, J.; Grips, V. K. W. *Surf. Coat. Technol.* **2012**, *208*, 92−100.
(39) Liu, X.; Chu, P. K.; Ding, C. *Mater. Sci. Eng., R* **2004**, *47*, 49−121.
(40) Sampath, S.; Herman, H. *J. Therm. Spray Technol.* **1996**, *5*, 445−456.
(41) Moss, M. *Acta Metall.* **1968**, *16*, 321−326.
(42) Schneider, G. B.; Perinpanayagam, H.; Clegg, M.; Zaharias, R.; Seabold, D.; Keller, J.; Stanford, C. *J. Dent. Res.* **2003**, *82*, 372−376.
(43) Wong, M.; Eulenberger, J.; Schenk, R.; Hunziker, E. *J. Biomed. Mater. Res.* **1995**, *29*, 1567−1575.
(44) Flemming, R. G.; Murphy, C. J.; Abrams, G. A.; Goodman, S. L.; Nealey, P. F. *Biomaterials* **1999**, *20*, 573−588.
(45) Ni, S.; Chang, J.; Chou, L.; Zhai, W. *J. Biomed. Mater. Res., Part B* **2007**, *80*, 174−183.
(46) Lozano, D.; Feito, M. J.; Portal-Núñez, S.; Lozano, R. M.; Matesanz, M. C.; Serrano, M. C.; Vallet-Regí, M.; Portolés, M. T.; Esbrit, P. *Acta Biomater.* **2012**, *8*, 2770−2777.
(47) Li, P.; Ohtsuki, C.; Kokubo, T.; Nakanishi, K.; Soga, N.; de Groot, K. *J. Biomed. Mater. Res.* **1994**, *28*, 7−15.
(48) Xue, W.; Liu, X.; Zheng, X.; Ding, C. *Surf. Coat. Technol.* **2005**, *200*, 2420−2427.
(49) Zreiqat, H.; Ramaswamy, Y.; Wu, C.; Paschalidis, A.; Lu, Z.; James, B.; Birke, O.; McDonald, M.; Little, D.; Dunstan, C. R. *Biomaterials* **2010**, *31*, 3175−3184.
(50) Liu, X.; Tao, S.; Ding, C. *Biomaterials* **2002**, *23*, 963−968.
(51) Shie, M. Y.; Ding, S. J.; Chang, H. C. *Acta Biomater.* **2011**, *7*, 2604−2614.
(52) Sun, J.; Wei, L.; Liu, X.; Li, J.; Li, B.; Wang, G.; Meng, F. *Acta Biomater.* **2009**, *5*, 1284−1293.
(53) Zinelis, S.; Tsetsekou, A.; Papadopoulos, T. *J. Prosthet. Dent.* **2003**, *90*, 332−338.
(54) Singh, S. P.; Pal, K.; Tarafder, A.; Das, M.; Annapurna, K.; Karmakar, B. *Bull. Mater. Sci.* **2010**, *33*, 33−41.
(55) Manning, W. R.; Hunter, O.; Calderwood, J. R. F. W.; Stacy, D. W. *J. Am. Ceram. Soc.* **1972**, *55*, 342−347.
(56) Li, C. L.; Zhao, H. X.; Takahashi, T.; Matsumura, M. *Mater. Sci. Eng., A* **2001**, *308*, 268−276.
(57) Pinto, P.; Ferreira, M. G. S.; Carmezim, M. J.; Montemor, M. F. *Electrochim. Acta* **2011**, *56*, 1535−1545.
(58) Diler, E.; Rioual, S.; Lescop, B.; Thierry, D.; Rouvellou, B. *Thin Solid Films* **2012**, *520*, 2819−2823.
(59) Ahmed, N. M.; Selim, M. M. *Pigm. Resin Technol.* **2005**, *34*, 256−264.